ISSN (Print) 1226-1750
ISSN (Online) 2233-6656
Journal of Magnetics 19(4), 327-332 (2014) http://dx.doi.org/10.4283/JMAG.2014.19.4.327

Microstructural Change and Magnetic Properties of Nanocrystalline Fe-Si-B-Nb-Cu Based Alloys Containing Minor Elements

Seul-Ki Nam, Sun-Gyu Moon, Keun Yong Sohn, and Won-Wook Park*

Department of Nano System Engineering, Inje University, Gyungnam 621-749, Korea

(Received 30 July 2014, Received in final form 18 December 2014, Accepted 19 December 2014)

The effect of minor element additions (Ca, Al) on microstructural change and magnetic properties of Fe-Nb-Cu-Si-B alloy has been investigated, in this paper. The Fe-Si-B-Nb-Cu(-Ca-Al) alloys were prepared by arc melting in argon gas atmosphere. The alloy ribbons were fabricated by melt-spinning, and heat-treated under a nitrogen atmosphere at 520-570°C for 1 h. The soft magnetic properties of the ribbon core were analyzed using the AC B-H meter. A differential scanning calorimetry (DSC) was used to examine the crystallization behavior of the amorphous alloy ribbon. The microstructure was observed by X-ray diffraction (XRD), transmission electron microscope (TEM) and scanning electron microscope (SEM). The addition of Ca increased the electrical resistivity to reduce the eddy current loss. And the addition of Al decreased the intrinsic magneto-crystalline anisotropy K_1 resulting in the increased permeability. The reduction in the size of the α-Fe precipitates was observed in the alloys containing of Ca and Al. Based on the results, it can be concluded that the additions of Ca and Al notably improved the soft magnetic properties such as permeability, coercivity and core loss in the Fe-Nb-Cu-Si-B base nanocrystalline alloys.

Keywords : nanocrystalline alloy, crystallization, soft magnetic cores, core loss, permeability

1. Introduction

Soft magnetic materials are presently required to exhibit good properties in a high frequency range. Recently, there has been a demand for enhanced performance from the materials used in miniaturized electromagnetic devices. These include the advanced soft magnetic materials used for magnetic heads, transformers, and other devices. The soft magnetic materials for advanced electronic devices especially need a high permeability, a low coercivity and a low core loss. Especially for the high frequency application, it is important to develop Co-free Fe-based soft magnetic materials with a lower core loss than commercialized Fe-Si-B-Nb-Cu nanocrystalline alloys. Besides, the core loss should be decreased more for the electronic devices for the high frequency of 1-100 kHz.

In 1988, Yoshizawa introduced a new class of iron based nanocrystalline alloys exhibiting superior soft magnetic behavior [1]. The particular about the new material was its ultrafine microstructure of α-Fe (Si) with grain sizes of 10-15 nm from which their soft properties lastly derive and after which they were named nanocrystalline. The material was produced by crystallization of an amorphous Fe-Si-B alloy with small additions of Cu and Nb, a hitherto somewhat unusual combination which proved to be key for the particular ultrafine grain structure and the associated soft magnetic properties. Only slightly partially crystallized amorphous Fe-based alloys were seen to offer eventual benefits over the amorphous state for certain high frequency applications [2, 3].

These materials are prepared using a rapid solidification technique such as melt spinning, which yields alloys in the form of amorphous ribbons. These optimally heat-treated amorphous ribbons have turned out to have nanocrystalline microstructures [4]. There have been numerous reports on Fe-based alloys with a fine uniform grain structure and an average grain size of about 10-20 nm [5, 6], which results in a zero value for the magnetostriction coefficient (λ_s) and crystalline magnetic anisotropy constant (K_1). The combination of small grain size and soft magnetic properties is surprising and fascinating from the classical point of view in magnetic engineering. The decrease of coercivity in the new nanocrystalline materials has to be well distinguished from superparamagnetic phenomena i.e., the well-known decrease of coercivity in small, isolated or weakly coupled particles due to thermal excitation [7-13].

*Corresponding author: Tel: +82-10-5525-3319
Fax: +82-55-320-3631, e-mail: wwpark@inje.ac.kr

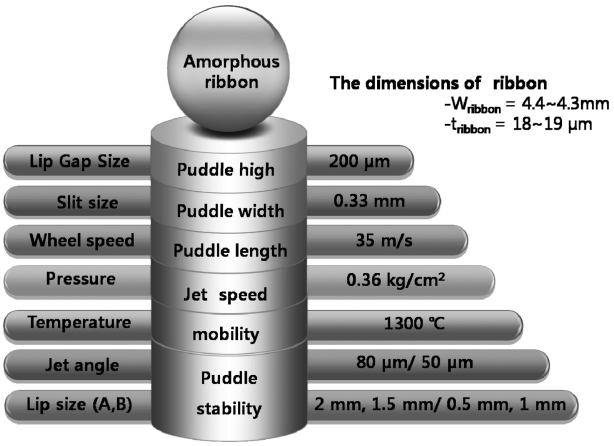

Fig. 1. Experimental conditions of melt-spinning for the Fe-based amorphous alloy ribbons.

Therefore, it is important to develop the Fe-based soft magnetic materials with a lower core loss and a higher saturation magnetic flux density than that of Fe-based amorphous and/or the commercialized nanocrystalline alloys. Further, the addition of Al causes the anisotropy and magnetostriction to become nearly zero, making oxidation surface [14]. The addition of Ca improves electrical resistivity [15]. On the basis of this viewpoint, the new alloy systems of Fe-Si-B-Nb-Cu, Fe-Si-B-Nb-Cu-Ca, and Fe-Si-B-Nb-Cu-Ca-Al nanocrystalline alloys were evaluated in this study to improve the magnetic properties with a high permeability and a low core loss at high frequency.

2. Experimental Procedure

Master alloy ingots were prepared by arc melting high-purity Fe(99.9%), B (99.9%), Si (99.9%) , Al (99.9%), Cu (99.9%) and pre-alloyed Si-Ca (30 wt%) in a Ti-gettered high-purity argon atmosphere. The ingots were re-melted two times and stirred by a magnetic beater to ensure its compositional homogeneity.

Ribbons with nominal compositions of

1. $Fe_{73}Si_{16}B_7Nb_3Cu_1$,
2. $Fe_{73}Si_{16}B7Nb_3Cu1$ + Ca (0.03 wt%),
3. $Fe_{73}Si_{16}B7Nb_3Cu1$ + Ca (0.03 wt%) + Al (0.5 wt%)

were prepared by a single roller melt-spinning apparatus under an argon atmosphere with a copper-wheel surface velocity of 35 m/s. The width and thickness of ribbons were with 4.3-4.4 mm and 18-19 μm, respectively.

These ribbon cores of Fe-based amorphous alloys were annealed to relieve the stress and crystallize the amorphous structure in the temperature range of 500-600°C for 1 h under nitrogen atmosphere. The crystalline structures of the samples were examined by X-ray diffraction (XRD). The microstructure of the ribbon was examined using the TEM, SEM and FESEM and the crystallization kinetics of the samples was examined with a differential scanning calorimeter (DSC). The magnetic properties such as the permeability, coercivity, and core loss of each core were measured using the AC *B-H* meter.

3. Results and Discussion

Table 1 shows chemical compositions of the Fe-based alloy ribbons. The Fe-based alloy ribbons were basically in amorphous state since the ribbons were prepared by rapid solidification.

The DSC (differential scanning calorimetry) results of the Fe-based alloy ribbons indicating T_g, T_{x1} and T_{x2} are shown in Fig. 2 and Table 2. Two distinct exothermic peaks on the curves indicate that the crystallization of every Fe-based alloy ribbons is through a two-step process. It should be noted that the first crystallization peak corresponds to the formation of α-Fe (Si) phase, and the second one corresponds to the formation of Fe borides, according to the previous investigations [16, 17]. It should also be noted that the onset temperature T_{x2} of the second crystallization process increase dramatically with adding the Ca content, while the onset temperature T_{x1} of the first crystallization process decrease dramatically with adding the Ca and Al content.

This phenomenon indicates that Al addition has effect on the amorphous formation ability and/or the formation of crystalline α-Fe (Si) phase due to the relatively decreasing T_{x1} with adding the Al content [18]. Lim *et al.* [19] and Zorkovska *et al.* [20] have found that the T_{x1} of $Fe_{73.5-x}Si_{13.5}B_9Cu_1Nb_3Al_x$ amorphous alloy decreases with increase of Al. Warren *et al.* [21] have investigated the spatial distribution of atoms in the nanocrystalline $Fe_{71.5}Si_{13.5}B_9Cu_1Nb_3Al_2$ alloy through a three-dimensional atom probe, and found the decrease of T_{x1} is attributed to the solution of Al into the Cu clusters, which enhances the precipitation of nanocrystals.

On the other hand, the increased T_{x2} with adding the Ca and Al content was also observed in Fe-Al-B ternary amorphous alloys [22], in which the crystallization temper-

Table 1. Chemical compositions of the melt spun Fe-based alloy ribbons (wt.%).

No.	Alloys	Fe	Si	B	Nb	Cu	**Ca**	**Al**
1	Fe-Si-B-Nb-Cu	83.14	8.52	1.85	5.29	1.19	**0.0042**	**0.0011**
2	Fe-Si-B-Nb-Cu-Ca	82.42	9.17	1.83	5.37	1.19	**0.022**	**0.002**
3	Fe-Si-B-Nb-Cu-Ca-Al	82.07	8.99	1.82	5.32	1.19	**0.028**	**0.58**

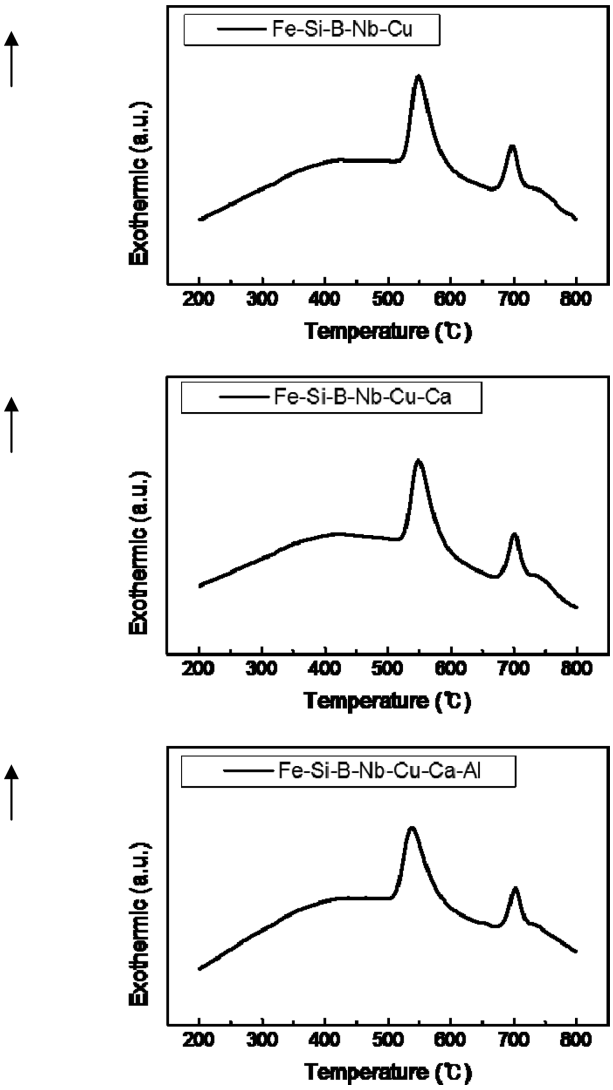

Fig. 2. DSC curves of Fe-based nanocrystalline soft magnetic alloys obtained on heating at a rate of 15 K/min.

ature corresponding to the formation of Fe borides increases with adding the Ca and Al content.

It is well known that crystallization of amorphous alloys is a nucleation/growth process, which is dominated by the diffusion of base metals. It can thus be concluded that the addition of Ca and Al might substantially inhibit the diffusion of B instead of Fe, since the formation temperature of single phase α-Fe (Si) decreases, while that of the Fe borides increases with increasing the Ca content.

Fig. 3 shows the XRD (X-ray diffraction) patterns of the fabricated the Fe-based alloy ribbons. As-spun ribbons of each composition were determined to be amorphous based on their XRD patterns. The patterns consist of broad halos without obvious detectable peaks, indicating the presence of a single amorphous phase within the detection limit of XRD.

The XRD patterns show that annealing at optimum

Table 2. Crystallization temperatures of Fe-based alloys determined by DSC results.

Alloy	Tg(°C)	Tx_1(°C)	Tx_2(°C)
Fe-Si-B-Nb-Cu	362.7	527.1	676.0
Fe-Si-B-Nb-Cu-Ca	324.1	527.5	682.2
Fe-Si-B-Nb-Cu-Ca-Al	325.9	513.7	684.0

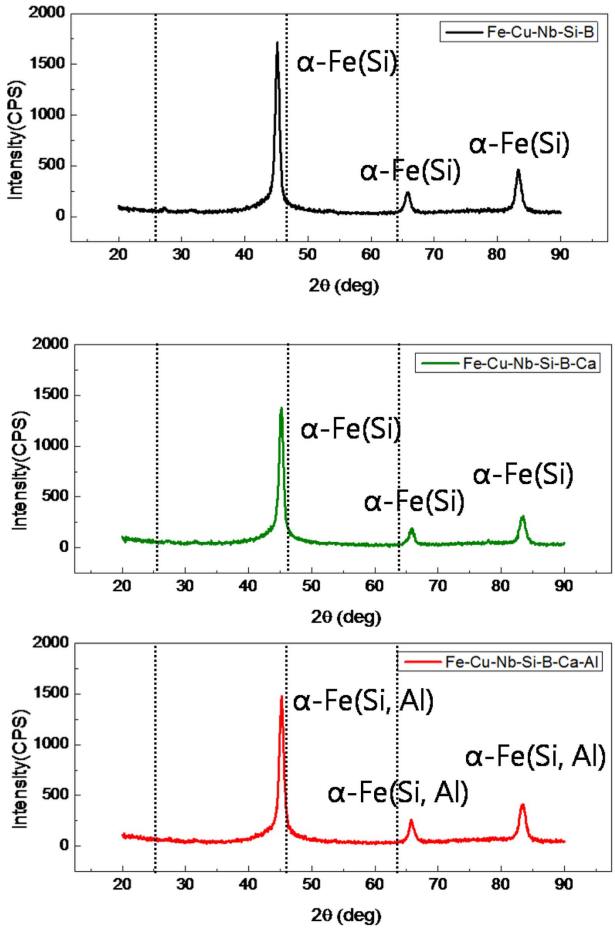

Fig. 3. (Color online) XDR results for Fe-based nanocrystalline alloys ribbon after optimum annealing.

annealing temperature (above the primary crystallization onset temperature) leads to the precipitation of α-Fe (Si) phase in the Fe-based alloy. Amorphous halos and overlap of sharp peaks in the XRD patterns can be seen, suggesting precipitation of the α-Fe (Si) crystals in the amorphous matrix due to annealing. B.J. Tate *et al.* have investigated the spatial distribution of atoms in the nanocrystalline $Fe_{71.5}Si_{13.5}B_9Cu_1Nb_3Al_2$ alloy, and found that Al is preferentially partitioned into the α-Fe (Si) nanocrystals and the Cu clusters over the amorphous matrix. Thus, the shift of peak is attributed to the solution of Al into the α-Fe (Si) [23]. Ca and Al alloying addition not only had a large effect on the crystallization temperatures, crystallization and

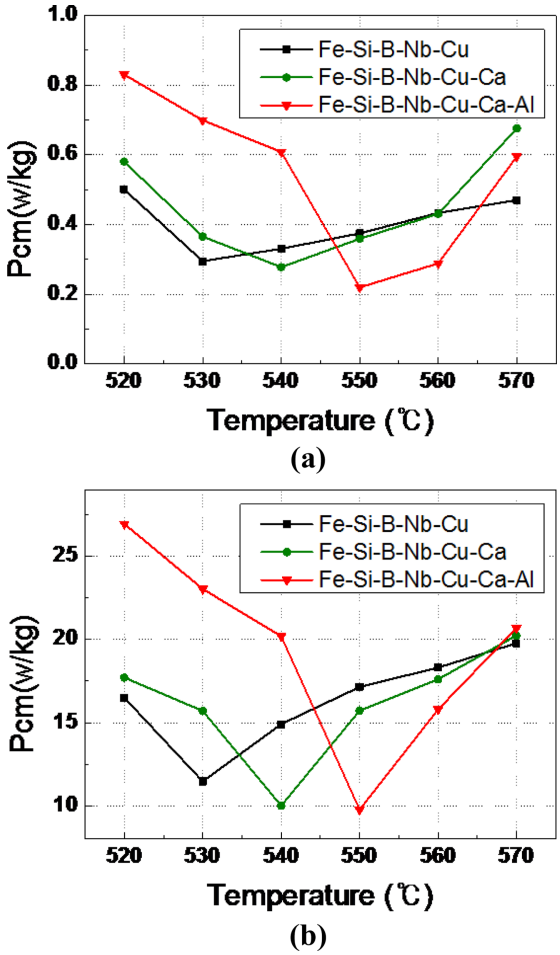

Fig. 4. (Color online) The core loss change as a function of annealing temperature, measured at (a) 0.1 T for 10 kHz, and (b) 0.1 T for 100 kHz.

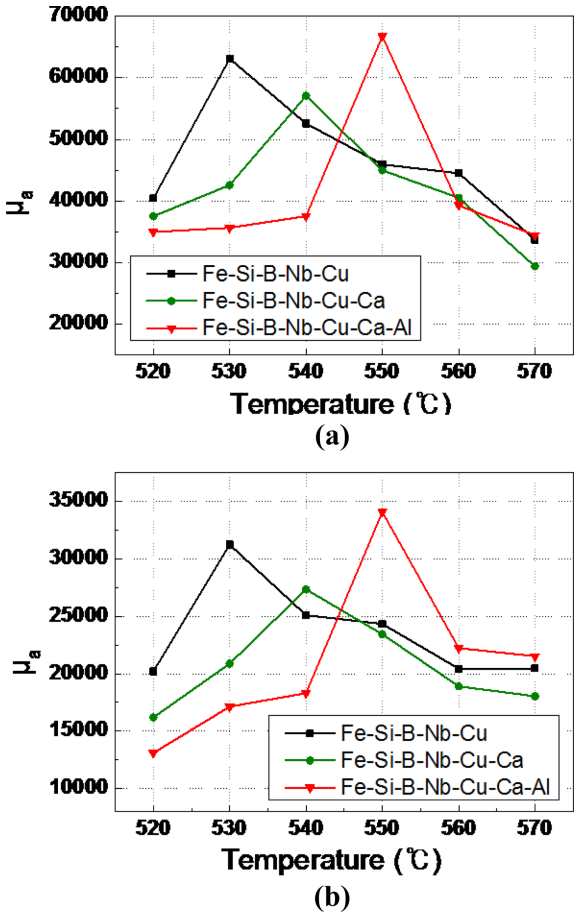

Fig. 5. (Color online) Applied field permeability of the Fe-based nanocrystalline soft magnetic alloys as a function of Annealing temperature, measured at (a) 0.1 T for 10 kHz, and (b) 0.1 T for 100 kHz.

microstructural evolution, but also affected the magnetic properties. The annealing temperature (T_a) dependences of the core loss (P_{cm}) are shown in Fig. 4(a) and (b), respectively. The core loss (P_{cm}) of the Fe-based ribbon cores with increasing annealing temperature was measured at 10 kHz and 100 kHz under an applied magnetic field of 0.1 T.

Ca was found in the grain boundary under the lower temperature, which prevented grain growth. However, when the temperature was increased, Ca seemed to form another compound that caused a decrease in the magnetic properties. As a result, at 540°C, the core loss of the Fe-Si-B-Nb-Cu-Ca alloy was rapidly decreased.

The lowest core loss at 10 kHz (P_{cm} = 0.2195 W/kg) was obtained from the Fe-based ribbon core made of the alloy containing Ca and Al at an annealing temperature of 550°C for 1 h, which was ~25% lower than that of the Fe-Si-B-Nb-Cu alloy core (P_{cm} = 0.295 W/kg).

The applied field permeability (μ_a) of Fe-based ribbon cores with increasing annealing temperature was measured

Table 3. The core loss and the permeability of the ribbon cores at each frequency (f = 1 kHz, 10 kHz, 100 kHz) at 0.1 tesla after the optimized annealing.

Alloy	Core loss (W/kg)			Permeability		
	1 kHz	10 kHz	100 kHz	1 kHz	10 kHz	100 kHz
Fe-Si-B-Nb-Cu	0.01547	0.295	11.46	79410	63100	31235
Fe-Si-B-Nb-Cu-Ca	0.01651	0.28765	10.155	69200	57050	27340
Fe-Si-B-Nb-Cu-Ca-Al	0.01483	0.2195	9.7625	86750	66740	34075

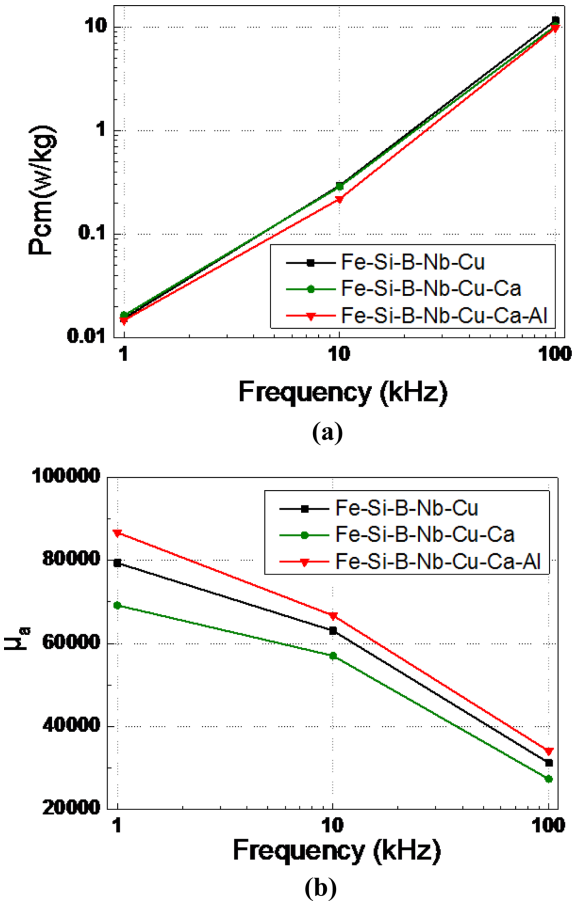

Fig. 6. (Color online) The magnetic properties of (a) core loss and (b) applied field permeability variations with frequency after the optimized annealing.

at 10 kHz and 100 kHz under 0.1 T, as shown in Fig. 5. The applied field permeability (μ_a) of the Fe-Si-B-Nb-Cu alloy was approximately 63,100 at 10 kHz, which was higher than that of the Ca-containing alloys (μ_a = 57050). However, the Fe-based alloy with Ca and Al showed the highest applied field permeability (μ_a) of 66,740 after annealing at 550°C for 1 h. The improvement in the soft magnetic properties of μ_a is considered to result from the reduction in the intrinsic magnetocrystalline anisotropy of the Ca and Al-added alloy ribbons (Table 3).

The variations of core loss and permeability with the frequencies after the optimized annealing were appeared in Fig. 6, indicating that the core loss increased and the permeability decreased with the increase of frequency.

Fig. 7 shows the transmission electron microscopy (TEM) micrographs of the Fe-Si-B-Nb-Cu-Ca-Al alloy ribbons after annealing at 550°C for 1 h. Materials with excellent soft magnetic properties could be obtained by the crystallization of the Fe-Si-B alloys with the addition of Cu and Nb. The addition of Cu and Nb led to the dispersion of ultrafine α-Fe(Si) nano-particles in an amorphous matrix,

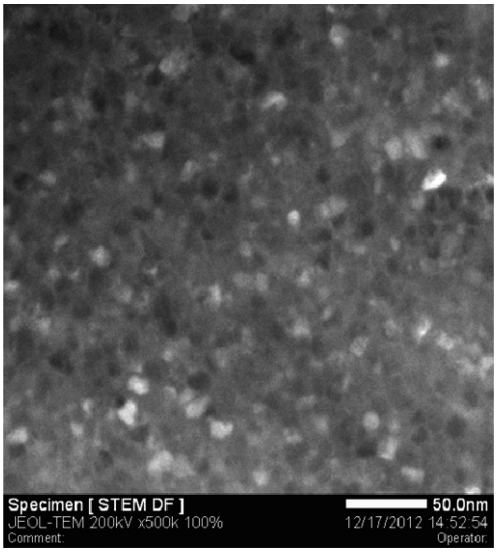

Fig. 7. TEM micrograph of Fe-Si-B-Nb-Cu-Ca-Al alloy ribbon after optimum annealing for 1 h at 550°C under N2 gas atmosphere.

which averaged out the magnetocrystalline anisotropy energy [24].

The grain size of the Fe-Si-B-Nb-Cu-Ca-Al alloy ribbon was finer than that of the Fe-Si-B-Nb-Cu alloy and Fe-Si-B-Nb-Cu-Ca alloy. This result may be attributed to the addition of the Ca and Al in the Fe-based alloy, which was probably even susceptible to the annealing temperature. Hence, it can be concluded that the addition of Ca and Al controlled the grain size. The Fe-Si-B-Nb-Cu-Ca-Al alloy ribbon consisted of ultrafine crystal grain size of 7-11 nm. This implied that the addition of Ca element could effectively suppress the grain growth in the nanocrystalline Fe-based alloy. And the effect of Al on the refinement of grains of the α-Fe (Si) solid solution phase is saturated at a very small amount of Al [14]. Since the microstructure of Fe-Si-B-Nb-Cu-Ca-Al alloy ribbon was almost the same as the commercialized Fe-Si-B-Nb-Cu Finemet alloy, the temperature dependence of magnetic properties such as Curie point of above 500°C is regarded to be excellent. Accordingly, it was necessary to obtain nanocrystalline grains of ~10 nm in order to rotate the magnetic domain easily [5, 6]. The magnetic behavior of soft magnetic nanocrystalline alloys depends strongly on the microstructure formed after the partial devitrification of the melt-spun amorphous ribbons.

4. Conclusions

1. The improvement in the soft magnetic properties of the permeability and the core loss for the alloys containing Ca and Al is considered to result from the reduction in the grain size of the α-Fe-Si solid solution phase in the Fe-Nb-

Cu-Si-B base nanocrystalline alloys.

2. The Ca addition to Fe-based nanocrystalline alloy was very effective to form the insulation layer of Ca oxide on the surface, resulting in the decrease of eddy current loss.

3. The improvement in the soft magnetic properties of permeability and the core loss is caused by the reduction in the intrinsic magnetocrystalline anisotropy of the Al-added alloy ribbons.

4. Accordingly, the additions of Ca and Al noticeably improved the soft magnetic properties as the toroidal ribbon core, which could meet the requirement for soft magnetic core in the frequency range of 1-100 kHz at 0.1 tesla.

Acknowledgement

This research was supported by Basic Science Research Program through the National Research Foundation of Korea (NRF) funded by the Ministry of Education, Science and Technology (2013 R1A1A01010423).

References

[1] Y. Yoshizawa, S. Oguma, and K. Yamauchi, J. Appl. Phys. **64**, 6044 (1988).
[2] R. Hasegawa, V. R. V. Ramanan, and G. E. Fish, J. Appl. Phys. **53**, 2276 (1982).
[3] G. Herzer and H. R. Hilzinger, J. Magn. Magn. Mater. **62**, 143 (1986).
[4] Y. Yoshizawa and K. Yamauchi, Mater. Trans., JIM **31**, 307 (1990).
[5] G. Herzer, IEEE Trans. Magn. **26**, 1397 (1992).
[6] G. Herzer, IEEE Trans. Magn. **25**, 3327 (1989).
[7] Pfeifer, F. and C. Radeloff, J. Magn. Magn. Mater. **19**, 190 (1980).
[8] F. E. Luborsky, J. Appl. Phys. **32**, 171S (1961).
[9] E. F. Kneller and H. Hawig, IEEE Trans. Magn. **27**, 3588 (1991).
[10] A. Manaf, R. A. Buckley, and H. A. Davies, J. Magn. Magn. Mater. **128**, 302 (1993).
[11] G. Herzer, In: Buschow, K. H. J., Handbook of magnetic materials, Amsterdam: Elsevier Science **10**, 415 (1997).
[12] R. Alben, J. J. Becker, and M. C. Chi, J. Appl. Phys. **49**, 1653 (1978).
[13] E. F. Kneller, Magnetism and Metallurgy, Eds. A. E. Berkowitz and E. Kneller, Academic Press: New York, London, 365 (1969).
[14] G. Herzer, J. Magn. Magn. Mater. **157**, 133 (1996).
[15] M. R. Kim, S. I. Kim, K. S. Kim, K. Y. Sohn, and W. W. Park, Metals and Materials International **18**, 185 (2012).
[16] T. H. Noh, M. B. Lee, H. J. Kim, and I. K. Kang, J. Appl. Phys. **67**, 5568 (1990).
[17] Y. Yoshizawa and K. Yamauchi, Mater. Sci. Eng. A **133**, 176 (1991).
[18] Y. Y. Sun and M. Song, J. Min. Metall. Sect. B-Metall. **48**(1), B:45 (2012).
[19] S. H. Lim, W. K. Pi, T. H. Noh, H. J. Kim and I. K. Kang, J. Appl. Phys. **73**, 6591 (1993).
[20] A. Zorkovská, J. Kováč, P. Sovák, P. Petrovič, and M. Konč, J. Magn. Magn. Mater. **215**, 492 (2000).
[21] P. J. Warren, I. Todd, and H. A. Davies, A. Cerezo, M. R. J. Bibbs, D. Kendall, R. V. Major, Scr. Mater. **41**, 1223 (1999).
[22] A. Inoue, A. Kitamura, and T. Masumoto, J. Mater. Sci. **16**, 1895 (1981).
[23] B. J. Tate, B. S. Parmar, I. Todd, H. A. Davies, M. R. J. Gibbs, and R. V. Major, J. Appl. Phys. **83**, 6335 (1998).
[24] A. K. Panda, B. Ravikumar, S. Basu, and A. Mitra, J. Magn. Magn. Mater. **260**, 70 (2003).